ORIGINAL ARTICLES

SPONTANEOUS RAMAN SPECTROSCOPY FOR INTRACRANIAL TUMORS DIAGNOSTICS EX VIVO

Romanishkin I.D.[1], Bikmukhametova L.R.[2], Savelieva T.A.[1,3], Goryaynov S.A.[4], Kosyrkova A.V.[4], Okhlopkov V.A.[4], Golbin D.A.[4], Poletaeva I.Yu.[4], Potapov A.A.[4], Loschenov V.B.[1, 2, 3]

[1]Prokhorov General Physics Institute of the Russian Academy of Sciences, Moscow, Russia
[2]OOO "BIOSPEC", Moscow, Russia
[3]National Research Nuclear University MEPhI (Moscow Engineering Physics Institute), Moscow, Russia
[4]N.N. Burdenko National Medical Research Center of Neurosurgery, Moscow, Russia

Abstract

Neurosurgery of intracranial tumors, especially of glial origin, is a non-trivial task due to their infiltrative growth. In recent years, optical methods of intraoperative navigation have been actively used in neurosurgery. However, one of the most widely used approaches based on the selective accumulation of fluorescent contrast medium (5-ALA-induced protoporphyrin IX) by the tumor cannot be applied to a significant number of tumors due to its low accumulation. On the contrary, Raman spectroscopy, which allows analyzing the molecular composition of tissues while preserving all the advantages of the method of fluorescence spectroscopy, does not require the use of an exogenous dye and may become a method of choice when composing a system for intraoperative navigation or optical biopsy.

This work presents the first results of using the principal component method to classify Raman spectra of human glioblastoma with intermediate processing of spectra to minimize possible errors from the fluorescence of both endogenous fluorophores and photosensitizers used in fluorescence navigation. As a result, differences were found in the principal component space, corresponding to tissue samples with microcystic components, extensive areas of necrosis, and foci of fresh hemorrhages. It is shown that this approach can serve as the basis for constructing a system for automatic intraoperative tissue classification based on the analysis of Raman spectra.

Keywords: glioblastoma, optical biopsy, spontaneous Raman scattering, principal component analysis.

For citations: Romanishkin I.D., Bikmukhametova L.R., Savelieva T.A., Goryaynov S.A., Kosyrkova A.V., Okhlopkov V.A., Golbin D.A., Poletaeva I.Yu., Potapov A.A., Loschenov V.B. Spontaneous Raman spectroscopy for intracranial tumors diagnostics *ex vivo*, *Biomedical Photonics*, 2020, vol. 9, no. 3, pp. 4–12 (in Russian). doi: 10.24931/2413–9432–2020–9–3–4–12.

Contacts: Romanishkin I.D., e-mail: igor.romanishkin@gmail.com

СПЕКТРОСКОПИЯ СПОНТАННОГО КОМБИНАЦИОННОГО РАССЕЯНИЯ ДЛЯ EX VIVO ДИАГНОСТИКИ ВНУТРИЧЕРЕПНЫХ ОПУХОЛЕЙ

И.Д. Романишкин[1], Л.Р. Бикмухаметова[2], Т.А. Савельева[1,3], С.А. Горяйнов[4], А.В. Косырькова[4], В.А. Охлопков[4], Д.А. Гольбин[4], И.Ю. Полетаева[4], А.А. Потапов[4], В.Б. Лощенов[1, 2, 3]

[1]Институт общей физики им. А.М.Прохорова Российской академии наук, Москва, Россия
[2]ООО «БИОСПЕК», Москва, Россия
[3]Национальный исследовательский ядерный университет «МИФИ», Москва, Россия
[4]НМИЦ нейрохирургии им.ак. Н.Н.Бурденко, Москва, Россия

Резюме

Нейрохирургия внутричерепных опухолей, особенно глиального происхождения, представляет нетривиальную задачу в силу их инфильтративного роста. В последние годы в нейрохирургии активно используются оптические методы интраоперационной навигации, однако один из наиболее широко распространенных подходов, основанный на селективном накоплении опухолью флуоресцентного контрастного вещества (5-АЛК индуцированного протопорфирина IX), не может быть применен для значимой части опухолей вследствие его низкого накопления. Напротив, спектроскопия комбинационного рассеяния, позволяющая проводить анализ молекулярного состава тканей с сохранением всех достоинств метода флуоресцентной спектроскопии, не требует при этом введения экзогенного красителя и может быть вариантом выбора при построении системы интраоперационной навигации или оптической биопсии.

В настоящей работе представлены первые результаты использования метода главных компонент для классификации спектров комбинационного рассеяния глиобластомы человека с промежуточной обработкой спектров для минимизации возможных ошибок от флуоресценции как эндогенных флуорофоров, так и фотосенсибилизаторов, используемых при флуоресцентной навигации. В результате были обнаружены различия в пространстве главных компонент, соответствующие образцам тканей с микрокистозными компонентами, обширными участками некрозов, фокусами свежих кровоизлияний. Показано, что данный подход может послужить основой для построения системы автоматической интраоперационной классификации тканей на основе анализа спектров комбинационного рассеяния.

Ключевые слова: глиобластома, оптическая биопсия, спонтанное комбинационное рассеяние, метод главных компонент.

Для цитирования: Романишкин И.Д., Бикмухаметова Л.Р., Савельева Т.А., Горяйнов С.А., Косырькова А.В., Охлопков В.А., Гольбин Д.А., Полетаева И.Ю., Потапов А.А., Лощенов В.Б. Спектроскопия спонтанного комбинационного рассеяния для *ex vivo* диагностики внутричерепных опухолей // Biomedical Photonics. – 2020. – Т. 9, № 3. – С. 4–12 doi: 10.24931/2413–9432–2020–9–3–4–12.

Контакты: Романишкин И.Д., e-mail: igor.romanishkin@gmail.com.

Introduction

The main problems of intracranial tumor neurosurgery are related to the complexity of tumor border demarcation due to the peculiarities of their growth. Glial tumors are known to propagate into the healthy white matter of the brain as tumor cells move along the blood vessels and nerve tracts due to the friendly microenvironment formed by the tumor-recruited immunecompetent cells. Such infiltration into healthy tissue makes radical resection impossible without creating a significant neurological deficit for the patient. In this regard, various intraoperative navigation methods have been actively used in neurosurgery in recent years, allowing for the most accurate differentiation of tumor and normal tissues, among which the optical technologies are particularly distinguished due to their efficiency and non-invasiveness. It is well known that protoporphyrin IX induced by 5-aminolevulinic acid is used for intraoperative navigation in glioblastoma surgery [1, 2]. Recently, many other methods for determining tumor borders have been investigated, including quantitative exogenous fluorescence analysis [3, 4], endogenous fluorescence lifetime imaging [5–7], optical coherence tomography (OCT) [8], hyperspectral imaging [9], and Raman scattering spectroscopy (RSS) [10, 11]. Each of these methods has its advantages, but RSS stands out among them as it allows for direct analysis of the molecular composition of the studied tissues without introducing any dyes, which leads to additional interest in this method as a diagnostic procedure which can determine tumor tissues characterized by a low level of accumulation of fluorescent markers, for example, tissues of benign glial tumors.

The first results of an RSS-based brain tumor analysis were obtained by K. Tashibu [12]. The author investigated the relative water concentration in normal and edematous brain tissues of rats by analyzing the CH and OH groups in the range of high wavenumbers. Cytotoxic and vasogenic models of brain edema in rats were also studied [13]. The works of A. Mizuno et al. [14, 15] provide the spectra of various brain tumors containing intense peaks characteristic for lipids. These early studies provided the impetus for further study of human brain tumors.

The development of fiber-optic probes [16] was the main factor that promoted the use of RSS for *in vivo* research. S. Koljenović et al. [17] examined pig brain tissue with the use of fiber-optic probes. As a result, it is shown that the analyzed Raman spectra of gray matter are dominated by bands associated with proteins, DNA, and phosphatidylcholine, while the white matter spectra are dominated by cholesterol and sphingomyelin.

Fiber-optic probes have also contributed to experimental studies of metastasis [18]. Melanoma cells were injected into the carotid artery of mice to cause brain metastasis. Serial sections were prepared from the whole mouse brain for analysis by Fourier spectroscopy and RSS methods. While metastatic melanoma cells were not detected with Fourier-infrared spectroscopy, RSS allowed for their detection with irradiation at a wavelength of 785 nm.

Ex vivo tissue studies provided essential information about the nature and composition of normal and tumor tissues. In the above study [15], the authors used RSS and Fourier spectroscopy to study various human brain tissue samples and showed that the spectra of normal but edematous, gray and white matter were similar to the spectra of normal gray and white matter in rats. It was observed that the spectra of gliomas, neurinomas, and neurocytomas are similar to those of gray matter in rats. In the study [19], 24 Raman maps were produced from unstained and unfixed sections of 20 glioblastoma tissue samples obtained from 20 patients. The necrotic tissues were found to have increased levels of cholesterol and cholesterol ester.

C. Krafft et al. [20, 21] performed brain tissue RSS for qualitative and quantitative analysis of lipid content.

Higher levels of lipids in normal tissues and higher hemoglobin content have been reported, and a lower ratio of lipids to proteins in intracranial tumors cases. Thus, RSS can be used to differentiate between normal and tumor tissues, as well as to determine the type and degree of malignancy of the tumor.

Due to the new facts about the relative content of lipids in brain tumors, Raman spectra of lipid extracts from seven human tissue samples were obtained [22]. Glioma tissues were characterized by increased water content and reduced lipid content, the results being consistent with the data obtained in the study of pig tissues.

Raman scattering (RS) was used to discover that the ratio of phosphatidylcholine to cholesterol is higher in gliomas compared to healthy tissues. The use of RSS helped differentiate brain tumors in children from normal brain tissue and distinguish similar types of tumors from each other [23].

Some works related to intraoperative *in vivo* studies of brain tumors have been published recently. As mentioned earlier, surgical resection in the case of intracranial tumors is challenging: any residual tumor cells can lead to a relapse, while healthy tissue removal can lead to cognitive impairment. Thus, early resection, as well as maintaining the functional status of patients, are crucial to achieving optimal results.

In a study involving 10 patients [24], the authors obtained real-time Raman spectra of healthy brain tissues, tumors, and necrotic tissues in vivo in real-time mode. Another study [10] shows differences in the Raman spectra between normal and tumor tissues in terms of the position of peaks of phospholipids, proteins, and nucleic acids.

The effectiveness of RSS was compared with that of MRI, which is a standard imaging method [25]. It is crucial to recognize that modern imaging technologies, including standard MRI, do not allow for the detection of distant invasive cells of glial brain tumors, since this restriction significantly reduces the effectiveness of surgical treatment of glioma. The authors of the paper demonstrate that RSS can detect invasive tumor cells far beyond the tumor detected by MRI in humans during surgery. RSS detects an invasion at a distance of ~ 3.7 cm and ~ 2.4 cm outside the borders of the MRI contrast zone.

To sum up the above, it is possible to conclude that RSS is the option of choice for intraoperative navigation in neurosurgery of intracranial tumors, especially of glial origin. RSS has a high spatial resolution, high data collection rate, and high sensitivity to changes in the molecular composition of tissues. It can detect invasive tumor cells without slowing down the neurosurgical process and complement or replace MRI-guided neuronavigation as a method for determining tumor boundaries.

Materials and methods

A spectroscopic system consisting of a Raman-HR-TEC-785 Raman scattering spectrometer (StellarNet, USA), a narrow-band laser radiation source with a wavelength of 785 nm (the width at half the amplitude of the laser peak of 0.2 nm, power up to 500 mW) Ramulaser™ 785 (StellarNet, USA), and a fiber-optic confocal probe for laser radiation and Raman scattering signal delivery (fig. 1) was used in this study. The use of the probe made it possible to receive a signal from an area less than 0.5 mm in diameter on the sample surface. The spectrometer was controlled from a computer with the software developed by us that allows recording a series of Raman spectra. This system allows recording spectra in the range of 800–1000 nm, which corresponds to the range of Stokes shifts of 200–2750 $cm^{-1.}$ The spectral resolution of the system was 4 $cm^{-1.}$

The studied material was obtained during the removal of human intracranial tumors (4 patients diagnosed with glioblastoma multiforme) and provided by the N. N. Burdenko National Medical Research Center of Neurosurgery. The material was examined under two conditions: in the operating room immediately after removal, *ex vivo* (2 patients, 7 tissue samples), and in the biobank 2 hours after removal (3 patients, 6 samples). During its transfer from the operating room to the biobank, the material was stored in saline.

The Raman spectra of each sample were recorded in a series of 5 measurements, with subsequent averaging. The exposure time of each measurement was 30 seconds (a total of 2.5 minutes per series) due to the technical limitations of the spectrometer used. Before each series, the background was measured (a series of 5 spectra of 30 seconds each), with the laser turned off. The background signal and Raman spectrum were measured in a darkened room.

During preprocessing, the spectra were first averaged within each series to reduce the contribution of random noise to the resulting signal. The corresponding average background spectrum was then subtracted from the average Raman spectra to exclude errors caused by the measurement conditions.

The obtained spectra were characterized by a high intensity of fluorescence, which is a noise signal for the RSS and worsens its decoding properties. To exclude the fluorescence component from the recorded signal, the algorithm presented in the paper [26] was used (Fig. 2). The method uses a continuous wavelet transform to determine the position of sharp Raman peaks and subtract the smooth background signal. The resulting spectrum was smoothed by a third-order Savitzky–Golay filter.

One of the difficulties in characterizing a tissue sample from the Raman spectrum is due to the high dimensionality of the obtained spectra, i. e., a large number of significant Raman peaks from various organic compounds.

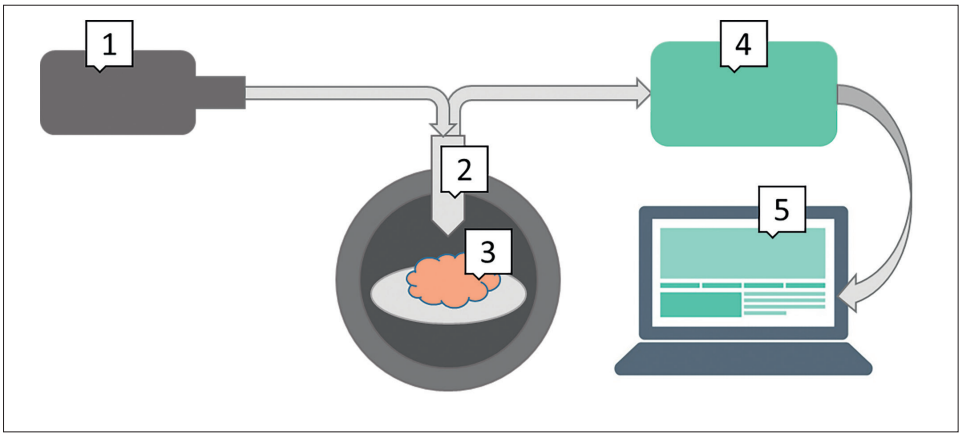

Рис. 1. Схема рабочей установки:
1. Источник узкополосного лазерного излучения с длиной волны 785 нм
2. Волоконно-оптический конфокальный зонд для доставки лазерного излучения и сигнала КР
3. Исследуемый образец биологической ткани
4. Спектрометр комбинационного рассеяния света
5. Компьютер со специальным программным обеспечением

Fig. 1. Working setup diagram:
1. Source of 785 nm narrow-band laser radiation
2. Fiber optic confocal probe for delivery of laser radiation and Raman signal
3. Sample of biological tissue
4. Raman spectrometer
5. Computer with special software

Raman spectra, unlike, for example, fluorescence spectra, are characterized by a large number of characteristic spectral lines, and their visual interpretation becomes a non-trivial task. To solve this problem, the principal component analysis (PCA) method was used as a dimensionality reduction method. Each spectrum represents a point on a hyperplane with a dimension corresponding to the number of values in the measured Raman spectrum. The PCA method rotates the coordinate system so that the axes lie along the data in the direction of the largest dispersion. With this rotation, each principal component is a linear combination of values along the original axes. At the same time, we do not need to consider those axes on which the data spread after such a rotation is minimal. This provides dimensionality reduction.

Results and discussion

Raman spectra of human glioma tissue specimens were obtained. Each of the samples was verified as glioblastoma multiforme WHO Grade IV. Foci of necrosis and vascular proliferation were found in all samples.

The Raman spectra obtained from each of the samples were processed according to the above methods. This allowed us to obtain spectra with minimized measurement errors and free from the fluorescent signal. As an example, fig. 3 shows the Raman spectra for patient K with the selection of the main peaks that characterize biomolecules whose content is increased in tumor tissues.

Patient K had the following distribution of material by biopsy: 1 – tumor, 20% necrosis; 2 – tumor, less than 30% necrosis; 3 – tumor, less than 40% necrosis, pronounced angiomatosis; 4 – tumor, up to 90% necrosis (of vascular genesis, being a conglomerate of thick-walled vessels and adjacent tumor tissue). The difference in the composition of the material is manifested in the difference in the intensity of the Raman peaks; however, the peaks that characterize glial tumors remain clearly visible (Fig. 3). Fig. 3 shows the significant contribution of cholesterol, protein, disaccharide, and nitrogenous bases into the process. As shown in the works of [19, 22], cholesterol can be associated with necrosis, which corresponds to the data of tumor specimen morphological studies.

The main components were analyzed in the spectral range of 900–1700 cm^{-1}, since it is in this region that the peaks characteristic of glial tumors predominate [27]. The main spectral features were observed for protein (1236, 1239 cm^{-1}), nitrogenous bases (1181, 1572 cm^{-1}), disaccharide (1461 cm^{-1}), deoxyribose (1430 cm^{-1}), and cholesterol (1085, 1296, 1032, 1451, 1659 cm^{-1}), acyl residues of lipids (1086 cm^{-1}) and phospholipids (1129 cm^{-1}).

The PCA result showed that the main differences (71% of the variance) are explained by the first two principal components (Fig. 4). If we consider the load spectra (how strongly the Raman signal affects the value of the principal component) of the first two components (Fig. 5), we can see a positive contribution of the Raman signal in the range of 1300–1450 cm^{-1} to the value of PC1,

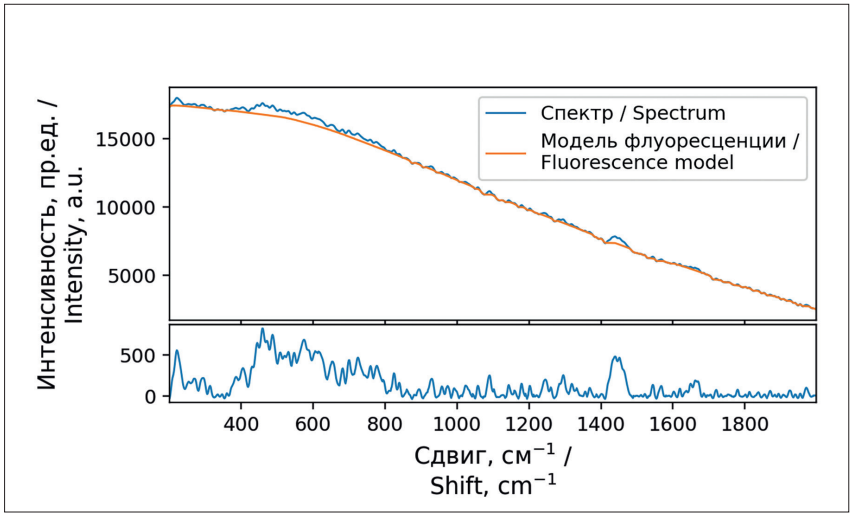

Рис. 2. Работа метода вычитания флуоресцентного сигнала из спектра КР. Сверху – измеренный спектр КР и построенная методом [26] модель гладкого спектра флуоресценции. Снизу – спектр КР без флуоресценции
Fig. 2. The work of the method of subtracting the fluorescent signal from the Raman spectrum. Above are the measured Raman spectrum and the smooth fluorescence spectrum model constructed by the method [26]. Below is the Raman spectrum without fluorescence

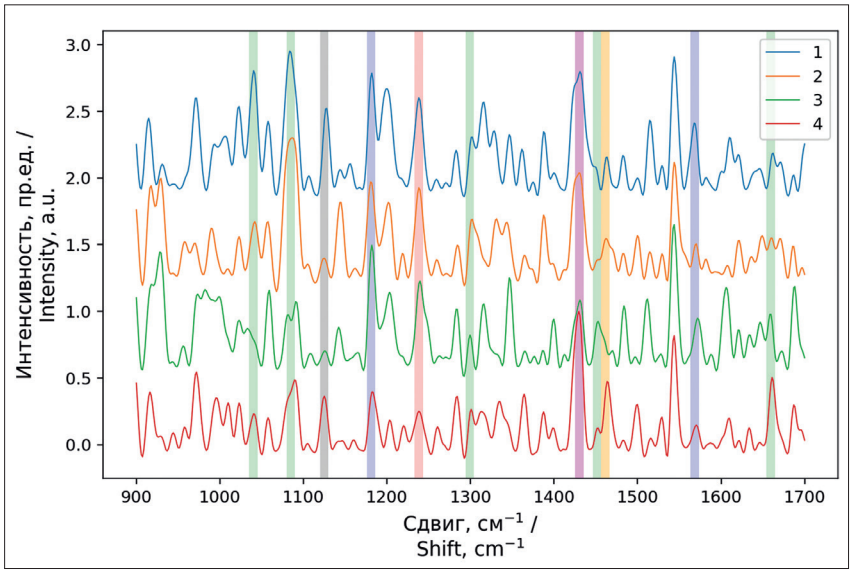

Рис. 3. Спектры КР образцов ткани пациента К. Значения интенсивности нормированы на максимум и смещены для удобства представления. Вертикальными полосами обозначены пики, характеризующие биомолекулы, содержание которых повышено в опухолевых тканях: белки (1236, 1239 см$^{-1}$, красный), азотистые основания (1181, 1572 см$^{-1}$, синий), дисахарид (1461 см$^{-1}$, желтый), дезоксирибоза (1430 см$^{-1}$, пурпурный), фосфолипид (1129 см$^{-1}$, серый), холестерин (1085, 1296, 1032, 1451, 1659 см$^{-1}$, зеленый)
Fig. 3. Raman spectra of patient K. tissue samples. Intensity values are normalized to a maximum and shifted for ease of presentation. The vertical lines indicate the peaks characterizing the biomolecules, the content of which is higher in tumor tissues: proteins (1236, 1239 cm^{-1}, red), nitrogenous bases (1181, 1572 cm^{-1}, blue), disaccharide (1461 cm^{-1}, yellow), deoxyribose (1430 cm^{-1}, magenta), and phospholipid (1129 cm^{-1}, gray), cholesterol (1085, 1296, 1032, 1451, 1659 cm^{-1}, green)

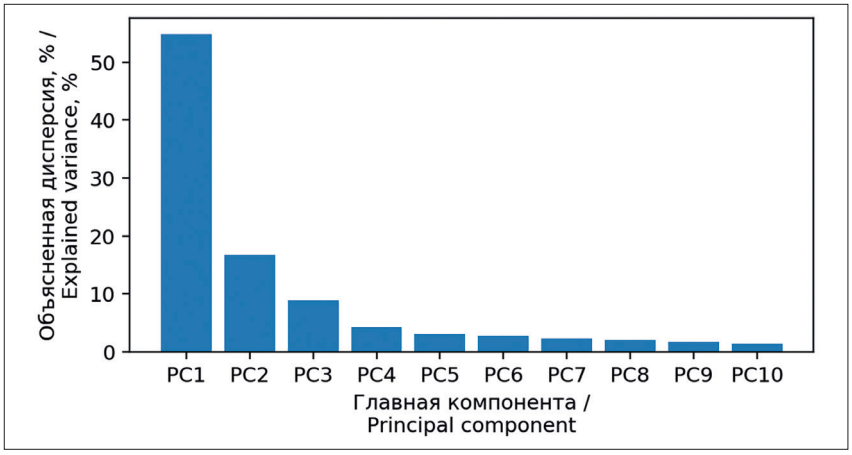

Рис. 4. Собственные значения главных компонент
Fig. 4. Eigenvalues of the principal components

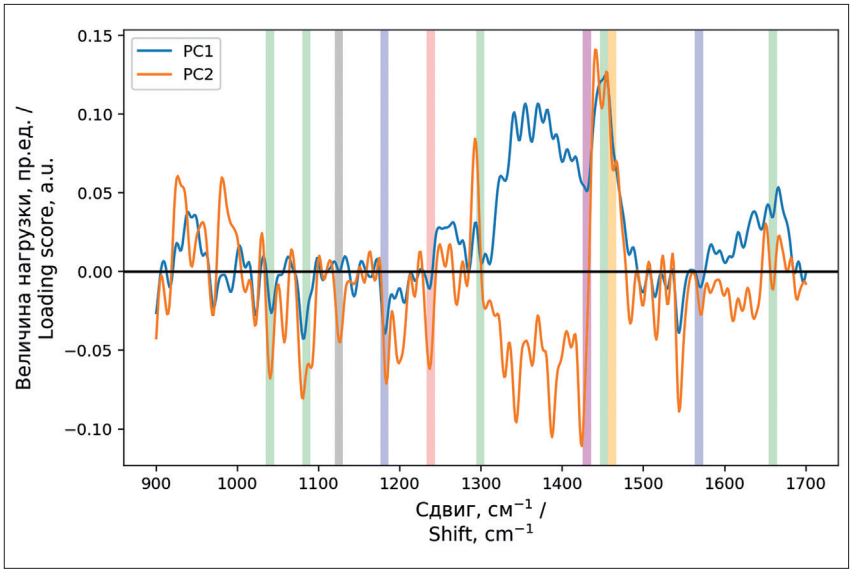

Рис. 5. Спектры нагрузки для первых двух главных компонент. Цветом выделены сдвиги, соответствующие биомолекулам, содержание которых повышено в опухолевых тканях (см. рис. 3)
Fig. 5. Loading score spectra for the first two principal components. Highlighted in color are the shifts corresponding to biomolecules, the content of which is higher in tumor tissues (see Fig. 3)

probably caused by high blood content. In this case, the PC2 value decreases with the increase of the signal from proteins, nitrogenous bases, and cholesterol (values at shifts of 1032 and 1085 cm^{-1}).

Distributions of the measured spectra from the first two principal components were obtained (Fig. 5, left). The material measured in the operating room forms a dense group in the third quarter of the PC1/PC2 coordinate plane. At the same time, no groups of measured samples are formed on the PC1/PC3 plane (Fig. 5, on the right), which suggests that the use of more than two main components when considering the measured data set is redundant. The Raman spectra of specimens from patient B, characterized by a massive hemorrhage, also lie in the negative PC1 range. The pathomorphological description of the tumor tissues of patient B showing the highest differences from the rest of the analysis by principal component method includes, in addition to the basic features of glioblastoma, such features as gliomezodermal scar tissue, and the presence of microcystic component, large areas of necrosis, and foci of fresh hemorrhage in the tumor. The pattern corresponds to glioblastoma with therapeutically induced changes.

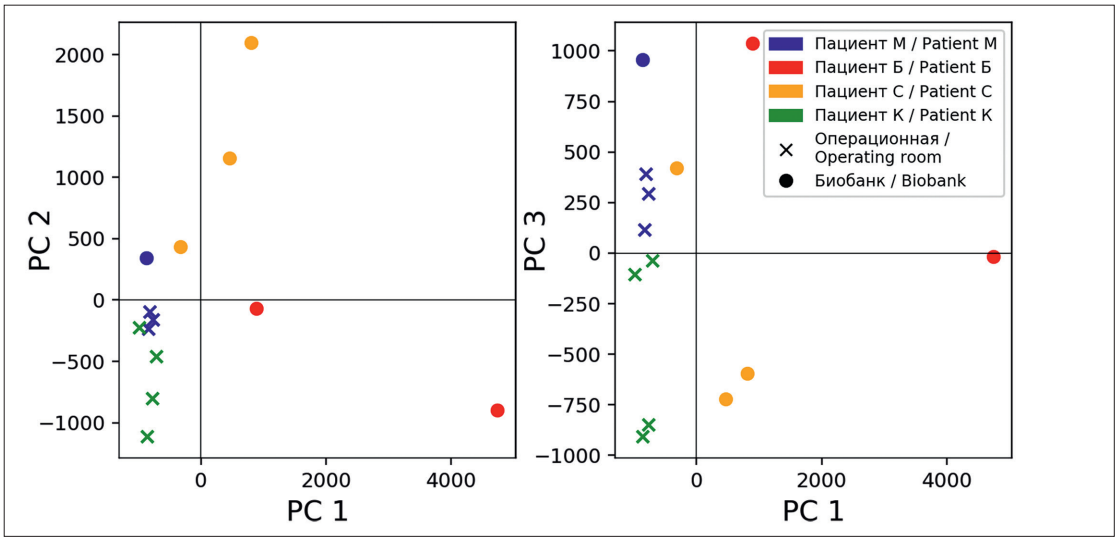

Рис. 6. Анализ главных компонент спектров КР образцов опухолевой ткани четырех пациентов, измеренных в операционной ex vivo и в биобанке
Fig. 6. PCA of the Raman spectra of tumor tissue samples from four patients, measured in the operating room ex vivo and in the biobank

The pathomorphological description of patient C's tissues also mentioned, against the background of the main features of multiform glioblastoma, microcystic structure, and foci of recent hemorrhages.

Conclusion

The paper presents the first results of the main component method for classification of spectra of glioblastoma tissue samples with intermediate processing of spectra to minimize possible errors due to fluorescence of both endogenous fluorophores and photosensitizers used in fluorescent navigation. There are differences in the principal components corresponding to tissue samples with microcystic components, extensive areas of necrosis, and foci of recent hemorrhages. A further set of data from different types of brain pathologies will enable clustering and analysis of the spectra [28] to build an intraoperative diagnostic system based on automatic Raman spectra analysis.

The study was carried out with the financial support of the Russian Foundation for Basic Research in the framework of research project No. 18–29–01062.

REFERENCES

1. Stummer W., Pichlmeier U., Meinel T., Wiestler O.D., Zanella F., Reulen H.J. Fluorescence-guided surgery with 5-aminolevulinic acid for resection of malignant glioma: a randomised controlled multicentre phase III trial, *Lancet Oncol*, 2006, vol. 7 (5), pp. 392–401.
2. Potapov A.A., Goriaïnov S.A., Loshchenov V.B., Savel'eva T.A., Gavrilov A.G., Okhlopkov V.A. Intraoperative combined spectroscopy (optical biopsy) of cerebral gliomas, *Zh. Vopr. Neirokhir. Im. N.N. Burdenko*, 2013, vol. 77 (2), pp. 3–10.
3. Valdes P.A., Jacobs V.L., Wilson B.C., Leblond F., Roberts D.W., Paulsen K.D. System and methods for wide-field quantitative fluorescence imaging during neurosurgery, *Opt. Lett.*, 2013, vol. 38 (15), pp. 2786.
4. Savelieva T.A., Loshchenov M.V., Borodkin A.V., Linkov K.G., Kosyrkova A.V., Goryajnov S.A., et al. Combined spectroscopic and video fluorescent instrument for intraoperative navigation when removing a glial tumor, *SPIE Photonics Europe*, 2020, vol. 11363. doi: 10.1117/12.2556064
5. Marcu L., Jo J.A., Butte P.V., Yong W.H., Pikul B.K., Black K.L., Thompson R.C. Fluorescence Lifetime Spectroscopy of Glioblastoma Multiforme, *Photochem. Photobiol.*, 2004., vol. 80 (1), pp. 98.

ЛИТЕРАТУРА

1. Stummer W., Pichlmeier U., Meinel T. et al. Fluorescence-guided surgery with 5-aminolevulinic acid for resection of malignant glioma: a randomised controlled multicentre phase III trial // Lancet Oncol. – 2006. – Vol. 7(5). – P. 392–401.
2. Potapov A.A., Goriaïnov S.A., Loshchenov V.B. Intraoperative combined spectroscopy (optical biopsy) of cerebral gliomas // Zh. Vopr. Neirokhir. Im. N. N. Burdenko. – 2013. – Vol. 77(2). – P. 3–10.
3. Valdes P.A., Jacobs V.L., Wilson B.C. et al. System and methods for wide-field quantitative fluorescence imaging during neurosurgery // Opt. Lett. – 2013. – Vol. 38(15). – P. 2786.
4. Savelieva T.A., Loshchenov M.V., Borodkin A.V. et al. Combined spectroscopic and video fluorescent instrument for intraoperative navigation when removing a glial tumor // SPIE Photonics Europe. – 2020. – Vol. 11363. DOI: 10.1117/12.2556064
5. Marcu L., Jo J.A., Butte P.V. et al. Fluorescence Lifetime Spectroscopy of Glioblastoma Multiforme // Photochem. Photobiol. – 2004. – Vol. 80(1). – P. 98.
6. Butte P.V., Mamelak A.N., Nuno M. et al. Fluorescence lifetime spectroscopy for guided therapy of brain tumors // Neuroimage. – 2011. – Vol. 54, Suppl. 1. – S125-S135.

6. Butte P.V., Mamelak A.N., Nuno M., Bannykh S.I., Black K.L., Marcu L. Fluorescence lifetime spectroscopy for guided therapy of brain tumors, *Neuroimage*, 2011, vol. 54, suppl. 1, s125–s135.
7. Kantelhardt S.R., Kalasauskas D., König K., Kim E., Weinigel M., Uchugonova A., Giese A. In vivo multiphoton tomography and fluorescence lifetime imaging of human brain tumor tissue, *J. Neurooncol.*, 2016., vol. 127 (3), pp. 473–482.
8. Kut C., Chaichana K.L., Xi J., Raza S.M., Ye X., McVeigh E.R., Rodriguez F.J. Detection of human brain cancer infiltration ex vivo and in vivo using quantitative optical coherence tomography, *Sci. Transl. Med.*, 2015, vol. 7 (292), 292ra100–292ra100.
9. Fabelo H., Ortega S., Lazcano R., Madroñal D., Callicó G.M., Juárez E. An Intraoperative Visualization System Using Hyperspectral Imaging to Aid in Brain Tumor Delineation, *Sensors*, 2018, vol. 18 (2), pp. 430.
10. Jermyn M., Mok K., Mercier J., Desroches J., Pichette J., Saint-Arnaud K., Intraoperative brain cancer detection with Raman spectroscopy in humans, *Sci. Transl. Med.*, 2015, vol. 7 (274), 274ra19–274ra19.
11. Brusatori M., Auner G., Noh T., Scarpace L., Broadbent B., Kalkanis S.N. Intraoperative Raman Spectroscopy, *Neurosurg. Clin. N. Am.*, 2017, vol. 28 (4), pp. 633–652.
12. Tashibu K. Analysis of water content in rat brain using Raman spectroscopy, No To Shinkei, 1990, vol. 42 (10), pp. 999–1004.
13. Kitajima T., Tashibu K., Tani S., Mizuno A., Nakamura N. Analysis of water content in young rats brain edema by Raman spectroscopy, *No To Shinkei*, 1993, vol. 45 (6), pp. 519–524. [in Japan.]
14. Mizuno A., Hayashi T., Tashibu K., Maraishi S., Kawauchi K., Ozaki Y. Near-infrared FT-Raman spectra of the rat brain tissues, *Neurosci. Lett.*, 1992, vol. 141 (1), pp. 47–52.
15. Mizuno A., Kitajima H., Kawauchi K., Muraishi S., Ozaki Y. Near-infrared Fourier transform Raman spectroscopic study of human brain tissues and tumours, *J. Raman Spectrosc.*, 1994, vol. 25 (1), pp. 25–29.
16. Beleites C., Geiger K., Kirsch M., Sobottka S.B., Schackert G., Salzer R. Raman spectroscopic grading of astrocytoma tissues: Using soft reference information, *Anal. Bioanal. Chem.*, 2011, vol. 400 (9), pp. 2801–2816.
17. Koljenović S., Schut T.C., Wolthuis R., Vincent A.J., Hendriks-Hagevi G., Santos L., et al. Raman spectroscopic characterization of porcine brain tissue using a single fiber-optic probe, *Anal. Chem.*, 2007, vol. 79 (2), pp. 557–564.
18. Krafft C., Kirsch M., Beleites C., Schackert G., Salzer R. Methodology for fiber-optic Raman mapping and FTIR imaging of metastases in mouse brains, *Anal. Bioanal. Chem.*, 2007, vol. 389 (4), pp. 1133–1142.
19. Koljenović S., Choo-Smith L.-P., Schut T.C.B., Kros J.M., van den Berge H.J., Puppels G.J. Discriminating vital tumor from necrotic tissue in human glioblastoma tissue samples by Raman spectroscopy, *Lab. Investig.*, 2002, vol. 82 (10), pp. 1265–1277.
20. Krafft C., Neudert L., Simat T., Salzer R. Near infrared Raman spectra of human brain lipids, *Spectrochim. Acta – Part A Mol. Biomol. Spectrosc.*, 2005, vol. 61 (7), pp. 1529–1535.
21. Krafft C., Sobottka S.B., Schackert G., Salzer R. Near infrared Raman spectroscopic mapping of native brain tissue and intracranial tumors, *Analyst*, 2005, vol. 130 (7), pp. 1070–1077.
22. Köhler M., Machill S., Salzer R., Krafft C. Characterization of lipid extracts from brain tissue and tumors using Raman spectroscopy and mass spectrometry, *Anal. Bioanal. Chem.*, 2009, vol. 393 (5), pp. 1513–1520.
23. Leslie D.G., Kast R.E., Poulik J.M., Rabah R., Sood S., Auner G.W., et al. Identification of pediatric brain neoplasms using raman spectroscopy, *Pediatr. Neurosurg.*, 2012. vol. 48 (2), pp. 109–117.
24. Desroches J., Jermyn M., Mok K., Lemieux-Leduc C., Mercier J., St-Arnaud K. et al. Characterization of a Raman spectroscopy probe system for intraoperative brain tissue classification, *Biomed. Opt. Express*, 2015, vol. 6 (7), pp. 2380.
7. Kantelhardt S.R. Kalasauskas D., König K., et al. In vivo multiphoton tomography and fluorescence lifetime imaging of human brain tumor tissue // J. Neurooncol. – 2016. – Vol. 127(3). – P. 473–482.
8. Kut C., Chaichana K.L., Xi J., et al. Detection of human brain cancer infiltration ex vivo and in vivo using quantitative optical coherence tomography // Sci. Transl. Med. – 2015. Vol. 7(292). – 292ra100.
9. Fabelo H., Ortega S., Lazcano R., et al. An Intraoperative Visualization System Using Hyperspectral Imaging to Aid in Brain Tumor Delineation // Sensors. – 2018. – Vol. 18(2). – P. 430.
10. Jermyn M., Mok K., Mercier J. Intraoperative brain cancer detection with Raman spectroscopy in humans // Sci. Transl. Med. – 2015. – Vol. 7(274). – 274ra19.
11. Brusatori M., Auner G., Noh T., et al. Intraoperative Raman Spectroscopy // Neurosurg. Clin. N. Am. – 2017. – Vol. 28(4). – P. 633–652.
12. Tashibu K. Analysis of water content in rat brain using Raman spectroscopy // No To Shinkei. – 1990. – Vol. 42(10). – P. 999–1004.
13. Kitajima T., Tashibu K., Tani S., et al. Analysis of water content in young rats brain edema by Raman spectroscopy // No To Shinkei. – 1993. – Vol. 45(6). – P. 519–524.
14. Mizuno A., Hayashi T., Tashibu K., et al. Near-infrared FT-Raman spectra of the rat brain tissues // Neurosci. Lett. – 1992. – Vol. 141(1). – P. 47–52.
15. Mizuno A., Kitajima H., Kawauchi K., et al. Near-infrared Fourier transform Raman spectroscopic study of human brain tissues and tumours // J. Raman Spectrosc. – 1994. Vol. 25(1). – P. 25–29.
16. Beleites C., Geiger K., Kirsch M., et al. Raman spectroscopic grading of astrocytoma tissues: Using soft reference information // Anal. Bioanal. Chem. – 2011. – Vol. 400(9). – P. 2801–2816.
17. Koljenović S., Schut T.C., Wolthuis R., et al. Raman spectroscopic characterization of porcine brain tissue using a single fiber-optic probe // Anal. Chem. – 2007. – Vol. 79(2). – P. 557–564.
18. Krafft C., Kirsch M., Beleites C., et al. Methodology for fiber-optic Raman mapping and FTIR imaging of metastases in mouse brains // Anal. Bioanal. Chem. – 2007. – Vol. 389(4). – P. 1133–1142.
19. Koljenović S., Choo-Smith L.-P., Schut T.C.B., et al. Discriminating vital tumor from necrotic tissue in human glioblastoma tissue samples by Raman spectroscopy // Lab. Investig. – 2002. – Vol. 82(10). – P. 1265–1277.
20. Krafft C., Neudert L., Simat T., et al. Near infrared Raman spectra of human brain lipids // Spectrochim. Acta - Part A Mol. Biomol. Spectrosc. – 2005. – Vol. 61(7). – P. 1529–1535.
21. Krafft C., Sobottka S.B., Schackert G. et al. Near infrared Raman spectroscopic mapping of native brain tissue and intracranial tumors // Analyst. – 2005. – Vol. 130(7). – P. 1070–1077.
22. Köhler M., Machill S., Salzer R., et al. Characterization of lipid extracts from brain tissue and tumors using Raman spectroscopy and mass spectrometry // Anal. Bioanal. Chem. – 2009. – Vol. 393(5). – P. 1513–1520.
23. Leslie D.G., Kast R.E., Poulik J.M., et al. Identification of pediatric brain neoplasms using raman spectroscopy // Pediatr. Neurosurg. – 2012. – Vol. 48(2). – P. 109–117.
24. Desroches J., Jermyn M., Mok K., et al. Characterization of a Raman spectroscopy probe system for intraoperative brain tissue classification // Biomed. Opt. Express. – 2015. – Vol. 6(7). – P. 2380.
25. Jermyn M., Desroches J., Mercier J., et al. Raman spectroscopy detects distant invasive brain cancer cells centimeters beyond MRI capability in humans // Biomed. Opt. Express. – 2016. – Vol. 7(12). – P. 5129.
26. Zhang Z.-M., Chen S., Liang Y.-Z., et al. An intelligent background-correction algorithm for highly fluorescent samples in Raman spectroscopy // J. Raman Spectrosc. – 2009. – Vol. 41(6). – P. 659–669.

25. Jermyn M., Desroches J., Mercier J., St-Arnaud K., Guiot M.-C., Leblond F., et al. Raman spectroscopy detects distant invasive brain cancer cells centimeters beyond MRI capability in humans, *Biomed. Opt. Express*, 2016, vol. 7 (12), pp. 5129.
26. Zhang Z.-M., Chen S., Liang Y.-Z., Liu Z.-X., Zhang Q.-M., Ding L.-X., et al. An intelligent background-correction algorithm for highly fluorescent samples in Raman spectroscopy, *J. Raman Spectrosc.*, 2009, vol. 41 (6), pp. 659–669.
27. Bikmukhametova L. R., Romanishkin I. A., Savelieva T. A., Skobeltsin A. S., Maklygina Yu. S., Loschenov V. B., et al. Spontaneous Raman Spectroscopy for Intracranial Tumor Diagnostics, *J. Phys. Conf. Ser.*, 2020, vol. 1439 (1), 012038.
28. Osmakov I. A., Savelieva T. A., Loschenov V. B., Goryajnov S. A., Potapov A. A. Cluster analysis of the results of intraoperative optical spectroscopic diagnostics in brain glioma neurosurgery, *Biomed. Photonics*, 2018, vol. 7 (4), pp. 23–34.

27. Bikmukhametova L.R., Romanishkin I.A., Savelieva T.A. et al. Spontaneous Raman Spectroscopy for Intracranial Tumor Diagnostics // J. Phys. Conf. Ser. – 2020. – Vol. 1439(1). – P. 012038.
28. Osmakov I.A., Savelieva T.A., Loschenov V.B., et al. Cluster analysis of the results of intraoperative optical spectroscopic diagnostics in brain glioma neurosurgery // Biomed. Photonics. – 2018. – Vol. 7(4). – P. 23–34.